A&A 635, A140 (2020)
https://doi.org/10.1051/0004-6361/201937062

Astronomy & Astrophysics

Short-term variability and mass loss in Be stars

V. Space photometry and ground-based spectroscopy of γ Cas*

C. C. Borre[1,2], D. Baade[2], A. Pigulski[3], D. Panoglou[4], A. Weiss[5], Th. Rivinius[6], G. Handler[7], A. F. J. Moffat[8], A. Popowicz[9], G. A. Wade[10], W. W. Weiss[11], and K. Zwintz[12]

[1] Stellar Astrophysics Centre, Department of Physics and Astronomy, Aarhus University, Ny Munkegade 120, 8000 Aarhus C, Denmark
e-mail: cborre@phys.au.dk
[2] European Organisation for Astronomical Research in the Southern Hemisphere (ESO), Karl-Schwarzschild-Str. 2, 85748 Garching b. München, Germany
e-mail: dbaade@eso.org
[3] Instytut Astronomiczny, Uniwersytet Wrocławski, ul. Kopernika 11, 51-622 Wrocław, Poland
[4] Observatório Nacional, Rua General Joé Cristino 77, São Cristóvão RJ 20921-400, Rio de Janeiro, Brazil
[5] Max-Planck-Institut für Astrophysik, Karl-Schwarzschild-Str. 1, 85748 Garching, Germany
[6] European Organisation for Astronomical Research in the Southern Hemisphere (ESO), Casilla 19001, Santiago 19, Chile
[7] Nicolaus Copernicus Astronomical Center, Polish Academy of Sciences, ul. Bartycka 18, 00-716 Warsaw, Poland
[8] Observatoire Astronomique du Mont Mégantic, Departement de Physique, Université de Montréal, CP 6128, Succursale: Centre-Ville, Montréal, QC H3C 3J7, Canada
[9] Silesian University of Technology, Institute of Automatic Control, Akademicka 16, Gliwice, Poland
[10] Department of Physics & Space Science, Royal Military College of Canada, PO Box 17000 Station Forces, Kingston, ON K7K 0C6, Canada
[11] Institute for Astrophysics, University of Vienna, Tuerkenschanzstrasse 17, 1180 Vienna, Austria
[12] Universität Innsbruck, Institut für Astro- und Teilchenphysik, Technikerstrasse 25, 6020 Innsbruck, Austria

Received 5 November 2019 / Accepted 6 February 2020

ABSTRACT

Context. Be stars are physically complex systems that continue to challenge theory to understand their rapid rotation, complex variability, and decretion disks. γ Cassiopeiae (γ Cas) is one such star but is even more curious because of its unexplained hard thermal X-ray emission.
Aims. We aim to examine the optical variability of γ Cas and thereby to shed more light on its puzzling behaviour.
Methods. We analysed 321 archival Hα spectra from 2006 to 2017 to search for frequencies corresponding to the 203.5 day orbit of the companion. Space photometry from the SMEI satellite from 2003 to 2011 and the BRITE-Constellation of nano-satellites from 2015 to 2019 were investigated in the period range from a couple of hours to a few days.
Results. The orbital period of the companion of 203.5 days is confirmed with independent measurements from the structure of the Hα line emission. A strong blue versus red asymmetry in the amplitude distribution across the Hα emission line could hint at a spiral structure in the decretion disk. With the space photometry, the known frequency of 0.82 d^{-1} is confirmed in data from the early 2000s. A higher frequency of 2.48 d^{-1} is present in the data from 2015 to 2019 and possibly in the early 2000s as well. A third frequency at 1.25 d^{-1} is proposed to exist in both SMEI and BRITE data. Seemingly, only a non-radial pulsation interpretation can explain all three variations. The two higher frequencies are incompatible with rotation.

Key words. stars: emission-line, Be – stars: oscillations – binaries: general – stars: individual: Gamma Cassiopeiae

1. Introduction

Classical Be stars are a subgroup of B-type stars with emission lines originating from a Keplerian decretion disk. These objects were first discovered by Secchi (1866) and were named Be stars for the spectral class B and emission lines. A widely accepted classification for classical Be stars is: "Non-supergiant B-type stars whose spectra have, or had at some time, one or more Balmer lines in emission" (Jaschek et al. 1981; Collins 1987). For a history of the classification and an overall review on Be stars, see Rivinius et al. (2013).

Be stars are rapid rotators with rotation velocities of ~75% of the critical rotation and above (Frémat et al. 2005; Meilland et al. 2012; Rivinius et al. 2013). The origin of the high rotation velocities of these objects is still a topic of debate. In binary systems, an explanation is spin-up due to angular momentum transfer from the companion (Kříž & Harmanec 1975; Pols et al. 1991; de Mink et al. 2013). For isolated stars, various mechanisms have been proposed such as angular momentum transfer from the core (Ekström et al. 2008; Granada et al. 2013), past interactions with an undetected companion, or

* Based on data collected by the BRITE-Constellation satellite mission that is designed, built, launched, operated, and supported by the Austrian Research Promotion Agency (FFG), the University of Vienna, the Technical University of Graz, the University of Innsbruck, the Canadian Space Agency (CSA), the University of Toronto Institute for Aerospace Studies (UTIAS), the Foundation for Polish Science & Technology (FNiTP MNiSW), and National Science Centre (NCN).

merger events (de Mink et al. 2011). It has been estimated that about one-third of Be stars are binaries (Abt & Levy 1978; Oudmaijer & Parr 2010). However, because of strong rotational broadening and frequent high intrinsic brightness and mass of B-type stars, it can be very challenging to detect a companion spectroscopically.

As discussed by Rímulo et al. (2018) and references therein, Be stars may undergo a surface-angular-momentum crisis as the core contracts and the outer parts spin up. The disk could, through viscosity, provide a way for the angular momentum to be dispersed so that the Be star is not rotationally disrupted (as originally envisioned by Struve 1931).

The formation of the disk is also an unsolved problem. It has been suggested that non-radial pulsations (NRPs) in combination with the rapid rotation cause mass ejections into the disk (e.g. Baade 1988). This is supported by the fact that nearly all Be stars display NRPs (see Rivinius et al. 2013, and references therein). Another suggestion is that tidal interactions with a companion can build the disk (Kříž & Harmanec 1975). However, the rarity of Be stars in binaries implies that such a model would only be able to explain a minority of the Be stars. Stellar winds were proposed but they are no longer a strong candidate after it was found that the mass-loss rate to the disk is an order of magnitude larger than the winds produced by a B-type star (Carciofi et al. 2012; Puls et al. 2008). Furthermore, Owocki et al. (1994) showed that it is not possible to form a Keplerian disk from winds. Magnetic fields were also a contender but this hypothesis was rejected owing to the lack of field detections in Be-type stars by the Magnetism in Massive Stars (MiMeS) survey (Wade et al. 2016).

After the mass has been ejected, a dust-free Keplerian disk is formed (Okazaki 1991; Papaloizou et al. 1992, to name a few). The most widely accepted theory for the disk is the viscous decretion disk model (Lee et al. 1991; Krtička et al. 2011). The disk behaves physically as an accretion disk if the time was reversed, that is the star ejects matter out into the disk instead of accreting it (Balbus 2003; Pringle 1981; Shakura & Sunyaev 1973). As long as the star keeps ejecting matter with appropriate angular momentum the disk is sustained. If the outbursts stop or become less frequent, the disk turns, within months to years, to an accretion disk and the inner parts reaccrete onto the star while the outer parts dissipate (Ghoreyshi et al. 2018). Because of its small size ($R_{\rm disk} \sim 10\,R_\star$; list in Rivinius et al. 2013, their Table 2) the disk varies on short timescales and can appear and disappear many times during the lifetime of the Be star. Furthermore, a spiral structure can form in the disk (Kato 1983; Okazaki 1991; Papaloizou et al. 1992).

Hα emission is the strongest optical emission line and its shape and evolution contain substantial information about the system. Horne & Marsh (1986) illustrated how different parts of the profile correspond to specific regions in the disk. For some binary Be stars, the Hα variation caused by a spiral arm has been observed to be phase-locked to the orbital motion of the companion (Štefl et al. 2007) while it is not for others. With simulations, Panoglou et al. (2016) demonstrate how, under suitable circumstances (circular and co-planar orbit with proper radius), the companion can induce or at least influence the spiral structure of the disk. The presence of a companion can also create resonances in the disk leading to a truncation as demonstrated by Okazaki et al. (2002). These authors showed that the disk becomes smaller than a disk unperturbed by a companion and that the density may be slightly larger because the disk is "squeezed" by the companion. This can appear as a flat top in the emission line structure because the outer parts of the disk, which contribute the most to the peaks at low velocities (Horne & Marsh 1986), are reduced in size.

The peak structure also depends on the viewing angle, that is the inclination of the disk. Rivinius et al. (2013, their Fig. 1) presents a sketch on how the structure can change from a wine bottle shape when viewed face-on (Hanuschik 1986) to an emission line with a narrow absorption core when viewed edge-on. Stars displaying lines with such narrow absorption cores are called shell stars (Hanuschik 1995; Rivinius et al. 1999). The shape of the line can change over time; see for example Hanuschik et al. (1996) for observations or Panoglou et al. (2018) for simulations on this.

In this paper, we provide an overview of γ Cas and a motivation of this work in Sect. 2 and a description of the observations in Sect. 3. The analysis is presented in Sect. 4, which is split into three parts based on the observing facility. In Sect. 5 we discuss the findings. A summary and conclusions are given in Sect. 6.

2. γ Cas

γ Cas (27 Cas, HR 264, HD 5394) is a B0.5 IVe star and is arguably the best known Be star. It was the first of its kind to be discovered by Secchi (1866) and was deemed the prototype for the class. It was later observed to exhibit hard X-ray emission (Jernigan 1976; White et al. 1982), which is unusual for early-type stars (Güdel & Nazé 2009). Furthermore, the X-ray flux is much lower than in Be-X-ray binaries (Nazé & Motch 2018). Recent work by Langer et al. (2020) suggests that the X-rays originate from the interaction between the wind from a He-star companion and the Be star disk or wind. More than a dozen other Be stars have been observed to have similar X-ray emission and this new class of stars is called the γ Cas analogues or γ Cas-like stars (Nazé & Motch 2018).

Using long-baseline optical interferometry, the inclination angle of the star's disk is observed to be around 45° with respect to the line of sight (e.g. Quirrenbach et al. 1997). Like all Be stars, γ Cas is a rapid rotator and rotates with near-critical velocity (Frémat et al. 2005).

γ Cas is a known binary system with an orbital period of 203.52(8) days (e.g. Harmanec et al. 2000; Miroshnichenko et al. 2002; Nemravová et al. 2012). The orbit is circular or has a very small eccentricity ($e < 0.03$). Signatures of the companion have not been observed directly but its presence is inferred from radial velocity measurements of the Be component. The mass of the Be primary is estimated to be 13−16 $M_\odot$ and the secondary between 0.5−1 $M_\odot$ (Harmanec et al. 2000; Nemravová et al. 2012).

γ Cas went through two shell phases in 1935-36 and 1939-40, both of which were preceded by a large outburst (e.g. Heard 1938; Baldwin 1940). It then appeared for a short time with no emission lines, that is no disk. In the second half of the 1940s the emission in the Balmer lines slowly returned and has been present ever since.

A few years ago, Henry & Smith (2012; and in the previous work by Smith et al. 2006) used the ground-based Automated Photometric Telescope[1] (APT), located in southern Arizona, to observe γ Cas from 1997−2011 in the V and B band. These authors found that the time series was dominated by slow two-to-three month variations on which a short periodic variation of 1.21 days (0.82 d^{-1}) was superimposed. This 1.21 day modulation varied in amplitude both in the blue and red wavelength range. During the end of the observation period, it almost disappeared. The period corresponds rather well with their radius and

[1] http://schwab.tsuniv.edu/t3.html

the near-critical rotational velocity estimate and it was accepted as the rotational period of the primary star in Henry & Smith (2012). They did not, however, state which property of the star is modulated by the rotation of the star.

There are also observations of migrating sub-features moving across photospheric absorption-line profiles (see e.g. Yang et al. 1988). It is still debated whether these features stem from NRPs or from co-rotating and absorbing cloudlets (Smith et al. 1998). A further overview of the observational history is given by Harmanec (2002).

The motivation for this new study of γ Cas is provided by the two phenomena that seem to make the supposedly prototypical Be star γ Cas different from other Be stars, namely the hard X-ray emission and apparent lack of NRPs. For an independent assessment of the effect of the companion on the Be star (cf. Langer et al. 2020), we used the Be Star Spectra database (BeSS) to analyse the structural change of the Hα line. This database is particularly suitable because of its long time baseline of spectra. Furthermore, we performed time series analyses of high-cadence space photometry to search for NRPs. For this, an obvious choice of instrument is the BRight Target Explorer (BRITE) because it observes bright stars repeatedly for half-year intervals and with multiple satellites and in two spectral passbands. A less common source of stellar photometry is the Solar Mass Ejection Imager (SMEI). However, as Goss et al. (2011) show for the bright Be star α Eridani, SMEI is very suitable for frequency detection in bright stars. Although the data from SMEI are rather noisy the long time baseline (∼nine years) makes up for the lower quality. In this way, SMEI and BRITE complement each other very well.

3. Observations and data reduction

3.1. Be Star Spectra Database (BeSS)

The BeSS Database[2] (Neiner et al. 2011) is ideal for studying spectral variations of Be stars on many timescales because it has a long time baseline of observations. The aim of this database is to collect spectra for all known Be stars and it is populated with data obtained by both professional and amateur observers.

The spectra in this analysis were selected using the following criteria: (1) a minimal wavelength range from 6550 to 6575 Å and (2) a resolving power of 15 000 and above. The BeSS query system uses the resolving power in the FITS headers, which is mostly automatically added by the respective data acquisition system. The observers can, however, also enter a number manually if something went wrong during the observations, for example, the calibration of the instrument (C. Neiner, priv. comm.). We used the BeSS entries of the resolving power but removed spectra that were obviously of lower resolution. A total of 389 spectra were downloaded on 22.11.17. After removal of spectra with saturated profiles or low resolving power, 371 spectra remained. The analysis was further limited to spectra observed after HJD 2453962.5 (15 Aug 2006) since there were very few spectra taken earlier than this date. This still means that the time span exceeds ∼11 years (2006−2017) and only 50 spectra were left out. Furthermore, all the spectra used by Harmanec et al. (2000) and most spectra used by Nemravová et al. (2012) have not (to our knowledge) been deposited in the BeSS Database. At most 13 of the 321 spectra in this work are also used by Nemravová et al. (2012). This makes the analysis performed in this study not only different from previous investigations but it is also applied to an independent dataset.

[2] http://basebe.obspm.fr

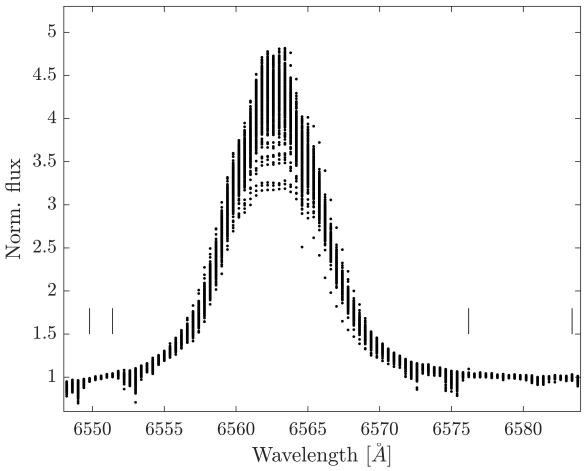

Fig. 1. 321 Hα profiles from the BeSS Database are binned in wavelength with a bin size of 0.4 Å. All profiles are normalised and the thin vertical lines indicate areas used for normalisation. The plot shows all profiles and they are therefore not resolved vertically. The Hα line is fairly stable compared to many other Be stars and roughly has a flat-top shape.

The spectra were corrected to the heliocentric reference frame, binned in wavelength to 0.4 Å, and normalised to the continuum. Caution was taken when normalising since some of the spectra did not extend over a very large wavelength range and therefore did not include a long stretch of continuum. Also, regions affected by strong telluric lines were not used to define the continuum. We selected two areas (one on each side of the Hα peak) and used a linear fit of the two regions to normalise the spectra. The result and normalisation regions can be seen in Fig. 1.

Each wavelength bin contains relative fluxes as a function of time (i.e. a time series). The time series were further prepared, now in a time domain, to search for periodic variations. The data in each wavelength bin were divided by a fitted second-degree polynomial to remove long-term (possibly non-periodic) trends. These trends can arise from several circumstances including the variety of instruments used to obtain the observations. Regardless, de-trending does not remove any of the shorter variations (i.e. shorter than five years). We then pre-whitened the time series of every wavelength bin to reduce the yearly variations. This was done by calculating the amplitude spectrum as described in Kjeldsen (1992) and Frandsen et al. (1995) and then removing the desired frequency. We pre-whitened for 1, 2, and 3 yr^{-1}. There was a strong yearly variation in the data; however, removal of the 2 and 3 yr^{-1} contributions had a smaller effect and did not change the outcome significantly.

3.2. Solar Mass Ejection Imager (SMEI)

The SMEI was launched on board the Coriolis satellite in 2003 to monitor space weather (Jackson et al. 2004). Its purpose was to detect Thomson-scattered sunlight from within the heliosphere volume. It was designed to have a lifetime of five years but was operated until September 2012. It had three cameras, each with a field of view of $3 \times 60\,\mathrm{deg}^2$, and was placed in a near-Earth orbit with a period of ∼100 min. The combination of the three cameras gave a 160° arc sweep of the sky. The aperture of each camera was approximately $1 \times 2\,\mathrm{cm}^2$.

To reach the required photometric precision when mapping the Thomson scattered light across the sky, all stars brighter than

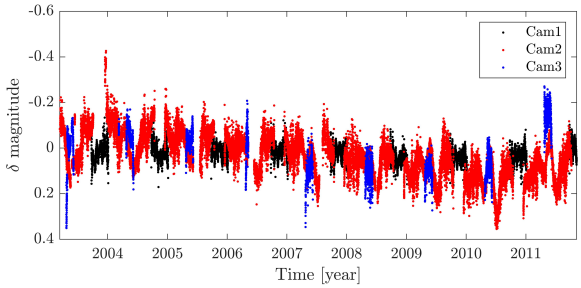

Fig. 2. Reduced data from SMEI Cameras 1 and 2. The data from Camera 3 are not reduced and only shown for comparison; they are not used in the time-series analysis.

Table 1. Overview of the SMEI observations.

Camera	JD start-end −2 450 000	No. of data points before reduction	No. of data points after reduction
1	2867.4–5833.3	10055	9787
2	2673.5–5810.1	29891	28855
3	2713.1–5681.2	4288	0

tenth magnitude had to be individually fitted and removed. The point spread function (PSF) used for the extraction had a full width of about 1 deg and varied in width depending on the path of the object through the field of view. This is a large diameter and attention should be paid when ascribing flux variations to a star because multiple bright stars can be located within the same PSF (Hick et al. 2007). The SIMBAD database (Wenger et al. 2000) lists one source brighter than a threshold of seventh magnitude within 0.6° of γ Cas. This is the triple system HD 5408, which has a magnitude of ~5.5, while γ Cas has a magnitude of ~2.5. Orbital periods for HD 5408 are known to be around 83 and 5 years (Tokovinin 1997).

In parallel with the SMEI observations, γ Cas was observed with the APT, which has a photometric aperture of at most 2 arcmin. Within this radius, there are no stars brighter than the 13th magnitude, which is not expected to influence the results. Since the 0.82 d^{-1} frequency, found in this work with SMEI, has already been detected with APT (Smith et al. 2006; Henry & Smith 2012; and HD 5408 is not included in the APT aperture) the 0.82 d^{-1} frequency is not due to HD 5408.

The University of California San Diego (UCSD) pipeline-extracted (Hick et al. 2005) stellar fluxes (in SMEI magnitudes; Buffington et al. 2007) are available on the web[3]. Unfortunately, the website only provides a single combined dataset for each star with no possibility of distinguishing between the different cameras. The data used in this work were kindly provided by B. Jackson (priv. comm. to DB) and contain information about the cameras, making it possible to separate the datasets. This turned out to be important as discussed below and in Sect. 4.2.

γ Cas was observed from 2004 to 2011 with all three cameras. The data were reduced using the pipeline but had to be further processed because of the large level of noise and large seasonal variations (see Fig. 2). This was done using a moving median assuming a normal distribution and a threshold of 4σ. The observation periods and number of data points can be seen in Table 1. Camera 3 was the most sunward camera, which was damaged during the mission from radiation from the sun. While Cameras 1 and 2 were kept at a temperature around −30°C to reduce noise, Camera 3 operated at temperatures between −2 and −15°C, which lowered the sensitivity (Webb et al. 2006). For this reason and because the number of data points from Camera 3 is relatively low, all the data from this camera have been discarded.

Lastly, the data were pre-whitened for 1, 2, 3, 4, 5, and 6 yr^{-1} and 1, 2, 3, and 4 d^{-1}. The reduced, pre-whitened and normalised time series is shown in Fig. 2. Data from Camera 3 are presented only for comparison and are not used in further calculations.

3.3. BRIght Target Explorer (BRITE)

The BRITE is a constellation of five nano-satellites operated by three countries, namely Austria, Canada, and Poland (Weiss et al. 2014). The first satellite to be launched in 2013 was named UniBRITE (UBr) followed by BRITE-Austria (BAb), BRITE-Lem (BLb), BRITE-Toronto (BTr), and BRITE-Heweliusz (BHr). A report on pre-launch and in-orbit tests can be found in Pablo et al. (2016). The "r" ("b") in these acronyms stands for a red 550−700 nm (blue 390−460 nm) filter. The satellites have a field of view of 20×24 deg^2 and a 3 cm aperture and similar to SMEI they were placed in a near-earth orbit with a period of about 100 min. The PSF varies across the field but has a size of about 3−6 $arcmin^2$ (Popowicz et al. 2017). At a radius of 6 arcmin from γ Cas there are no stars brighter than ~11th mag. The goal of these satellites is to acquire simultaneous and nearly continuous dual-broadband photometry of bright stars for up to half a year. In contrast to the SMEI project, the BRITE satellites are specifically designed to observe bright stars and the metadata are much more detailed.

The BRITE data were extracted using aperture photometry and were pipeline reduced prior to the reduction described below. A description of the pipeline reduction can be found in Popowicz et al. (2017) and is the same for all the observation runs presented in this work. Owing to slightly different set-ups (mostly resulting from field re-acquisitions) between the satellites, we further decorrelate and reduced each dataset individually. The reduction can also depend on the specific star requiring this individual computation. Furthermore, during an observing run, a single satellite can have different set-ups. These are then reduced separately and combined at the very end. The need for decorrelations and typical methods are further described in the official "cookbook" (Pigulski 2018). As suggested in the cookbook, we used orbital averages of the data points. This means that the Nyquist frequency is ~7.2 d^{-1} which is sufficient for our analysis. For each set-up, the mean magnitude is set to zero because the BRITE satellites only deliver relative photometry.

After the reduction, the data were pre-whitened for 1, 2, 3, 4, 5, and 6 yr^{-1} and 1, 2, 3, and 4 d^{-1}. This was done even though no significant peaks at these frequencies were seen in the amplitude spectra.

In Table 2 information about the BRITE data is given. The reduced and pre-whitened BRITE time series in context of SMEI and APT (Henry & Smith 2012) is shown in Fig. 3. The BRITE time series alone is presented in Fig. 4.

4. Results of the analysis

Similar to Sect. 3 this section is organised by observing facility. Some discussions of the frequencies are therefore repeated.

[3] http://smei.ucsd.edu/new_smei/data&images/stars/timeseries.html

Table 2. Overview of the BRITE observations.

Satellite name (acronym)	Orbital period [min]	Year	Contig. time [min]	JD start-end −2 457 000	Range in CCDT [°C]	No. of exposures	No. of TSA data points
BRITE-Austria (BAb)	100.4	2015	4.7–19.3	263.5–321.6	17.7–30.9	17349	501
		2016	5.8–14.6	608.3–751.5	16.2–29.1	24837	752
		2017	3.0–14.8	973.4–1133.6	17.9–33.8	13086	470
		2018	2.6–9.8	1339.9–1435.8	18.0–31.8	4569	121
BRITE-Lem (BLb)	99.6	2015	7.5–20.3	294.9–312.2	32.1–39.4	9910	163
BRITE-Heweliusz (BHr)	97.1	2015	4.1–19.6	266.4–313.3	8.5–20.8	5226	143
BRITE-Toronto (BTr)	98.2	2015	4.4–16.6	360.8–408.5	12.7–23.1	17111	632
		2018	5.4–10.9	1410.0–1505.5	16.0–26.5	32460	1027
UniBRITE (UBr)	100.4	2016	4.7–14.9	645.1–786.1	17.6–31.5	29934	838

Notes. Suffixes "r" and "b" refer to red and blue passbands, respectively. "Contig. time" denotes the typical contiguous time interval per orbit during which exposures were made. CCDT is the temperature of the detector. TSA (time series analysis) data points are the number of data points formed by an orbital average of the exposures and after data reduction.

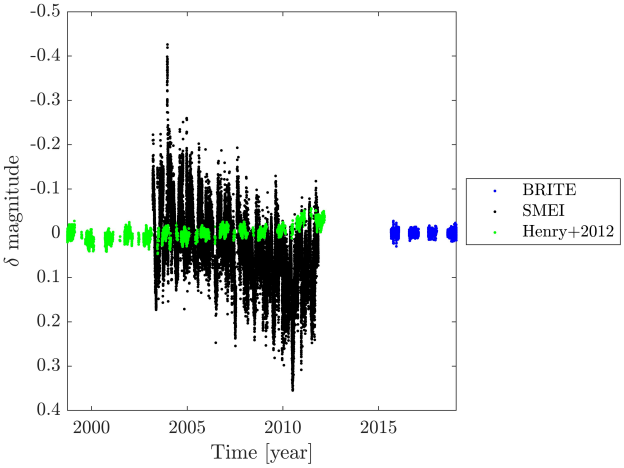

Fig. 3. Time series of BRITE (blue), SMEI (black), and APT (green) photometry. The mean magnitude of SMEI and BRITE is 0 by construct. The mean magnitude of the APT data has been shifted to zero compared to the data provided on the web. The APT data were analysed in detail by Henry & Smith (2012). The figure shows that the noise in the SMEI satellite data is significantly higher than in the APT and BRITE measurements.

4.1. Frequencies in BeSS spectra

The amplitude spectrum of the de-trended and pre-whitened BeSS data was calculated for all wavelength bins individually and is presented in Fig. 5. On top of the amplitude spectrum, an example of an Hα line is shown for easier cross identification between line structure and wavelength. The dash at ~6565 Å indicates a telluric line and this region should be interpreted with caution. Arrows point to frequencies of interest, which are discussed below.

The largest amplitude is denoted with arrow *a*. The wavelength bins between 6556 and 6560 as well as between 6565 and 6569 Å were fitted with a sinusoid resulting in a mean period of 202.9(5) days (uncertainty from standard deviation). This agrees with the known binary orbital period of 203.52(8) days that has been reported by others (see for example Harmanec et al. 2000; Nemravová et al. 2012). These papers measure the periods using the radial velocity of the emission line wings. As this method has already been used extensively on this star, we do not repeat it in this work. By examining the flux change in each wavelength bin (as is done in ths work) instead of the radial velocity, the structural change of the disk can be probed. This is due to the strong correlation between the structure of the Hα emission and that of the disk (Horne & Marsh 1986). The frequency is dominant in the wings because a shift in a flat top does not lead to a significant signal.

The blue versus red asymmetry of the amplitude in the wings is, on the other hand, a remarkable result. Panoglou et al. (2016) show simulations that demonstrate how the companion can induce or at least influence a spiral structure in the disk so that the rotation of the companion and the spiral becomes phase-locked. This asymmetry could, therefore, arise because of the observational difference between the concave and convex part of the spiral arm. For example, if the optical thickness of the gas is different in the denser front part of the spiral arm compared to the gas trailing behind it, the reprocessed light from the star is also different. Given a one-armed structure, one would equally often observe the back and front side of the spiral arm but at different luminosities. This would give an equal frequency of the two sides of the arm but with different amplitude, as is seen in Fig. 5. According to simulations, a two-armed structure could form (Panoglou et al. 2016) which could produce a signal at double the orbital frequency (arrow *b*, Fig. 5). We do not observe such a signal and we discuss why this might be the case in Sect. 5.1.

To check the robustness of the orbital signal, we split the data sample into two halves: by time and by randomly selecting the data. In all four cases, the orbital frequency is still visible although (naturally) not as prominent. The time series was folded with the orbital period and Fig. 6 shows that it is well defined and that the data are evenly distributed over the phases.

4.2. Frequencies in SMEI photometry

The SMEI data show slow trends (clearly seen in Fig. 3) that can affect the amplitude spectrum and we have therefore applied a high-pass filter to reduce their effects on the noise at higher frequencies. The amplitude spectra for Camera 1 and Camera 2 of the SMEI data can be seen in Fig. 7.

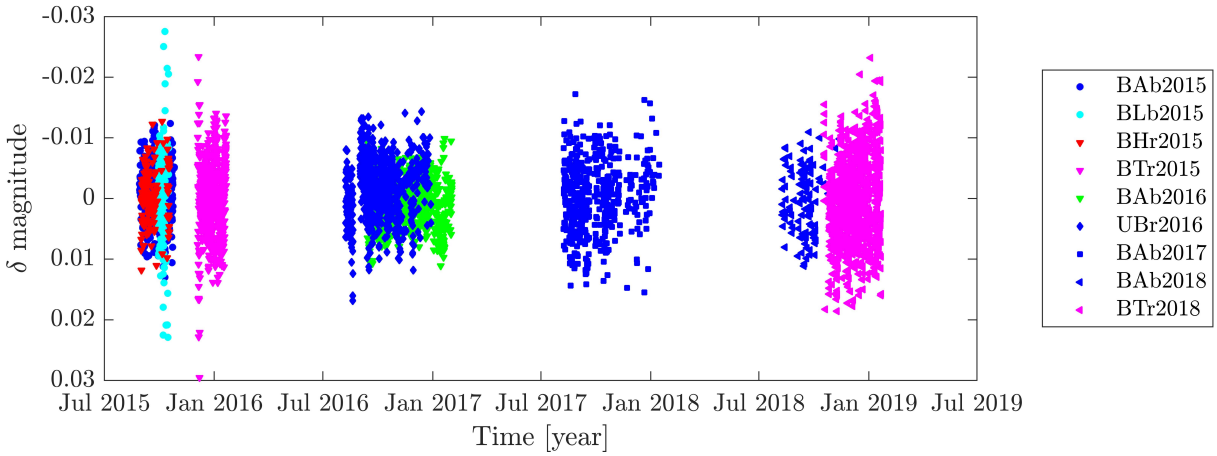

Fig. 4. Time series of BRITE photometry. The mean magnitude of the individual datasets is 0 by definition.

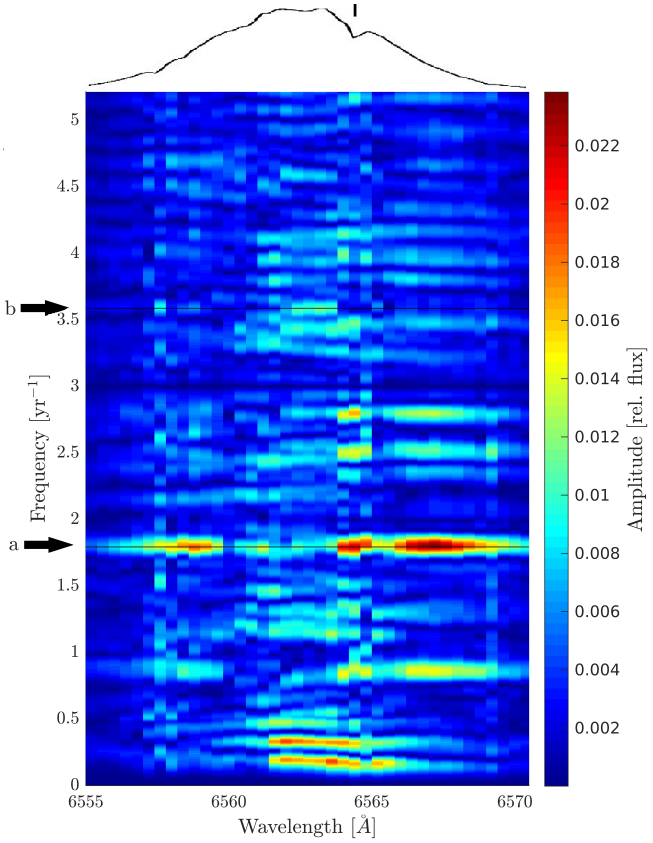

Fig. 5. Wavelength-resolved amplitude spectrum for γ Cas across the Hα profile. An example of the Hα profile is shown on top as reference. Arrows mark regions of interest: (*a*) stellar orbital frequency, (*b*) twice the stellar orbital frequency. The signature at ~6564.5 Å (marked on the profile) is caused by telluric contamination.

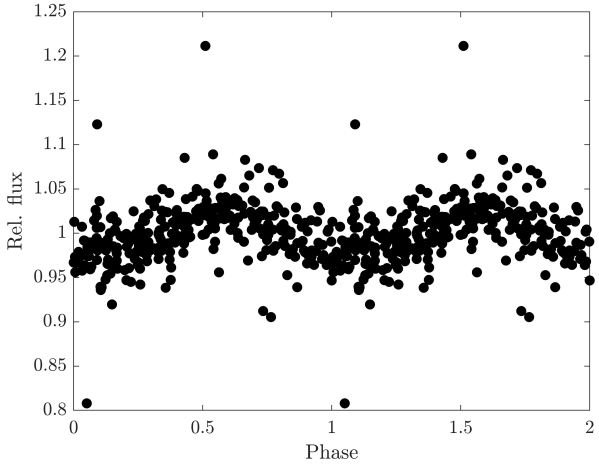

Fig. 6. Phase-folded time series of Hα fluxes at wavelength bin 6567.1 Å. The data are folded with the orbital period and are repeated for clarity.

It is clear that some of the major features correspond to 1, 2, and 3 d^{-1}, which have (most likely) nothing to do with the star but rather (the local environment of) the satellite or from light scattered off clouds and ice on Earth. These features are reduced through the pre-whitening process but they are not entirely gone. This could be because the pre-whitening is only done on one peak in the amplitude spectrum and its associated features in the window function. This means that even though the code takes the structure of the data into account, the signal is not perfectly sinusoidal and it might not be removed completely. It is, however, not important to remove all these features fully as long as one is careful not to attribute them to the star. We tested a more detailed pre-whitening (with more peaks removed), but it did not affect the detections of the stellar frequencies in any significant way.

In Camera 2 data there is a large bump at 2.3–2.4 d^{-1}. Such a bump is seen in many SMEI datasets (although not always at the same frequencies) and is, therefore, considered instrumental (Pigulski, priv. comm.).

The most significant non-instrumental signal in both spectra is at 0.82 d^{-1}. By combining the time series of the two cameras we obtain a time series with smaller gaps and a tighter constraint on the frequency. The amplitude spectrum from SMEI Cameras 1 and 2 combined is shown in Fig. 8. For frequency determination throughout the rest of this work, we use Period04 (Lenz & Breger 2005), which is the accepted standard in the field of stellar pulsation analysis. Period04 calculates uncertainties as described by Breger et al. (1999) and Montgomery & O'Donoghue (1999). Analysing the two datasets separately we obtain a frequency of 0.82200(2) d^{-1} for Camera 1 and 0.82217(2) d^{-1} for Camera 2. These frequencies agree within 4.3σ, which we accept as consistent because the uncertainties returned by Period04 assume normally distributed

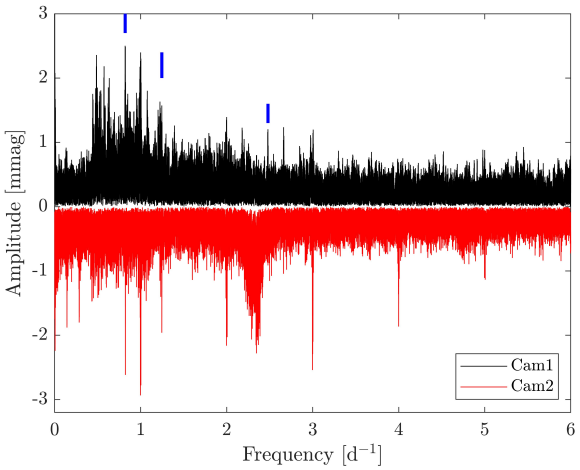

Fig. 7. Amplitude spectra of the two SMEI time series. The spectrum from Camera 2 has been flipped to negative values for clarity. Frequencies 0.82, 1.25, and 2.48 d^{-1} are denoted.

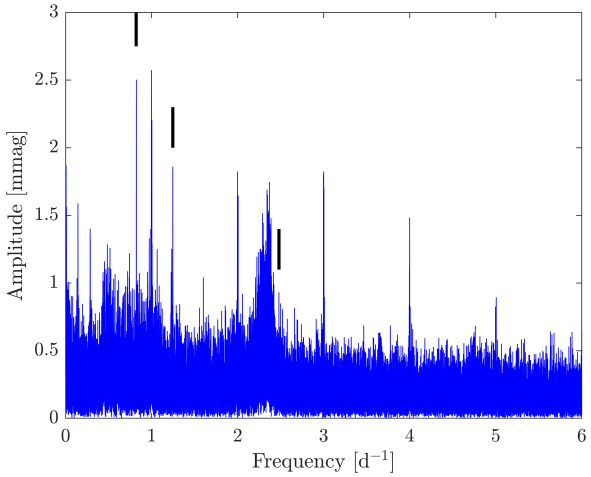

Fig. 8. Amplitude spectrum of the combined SMEI data (Camera 1 + Camera 2). Frequencies 0.82, 1.25, and 2.48 d^{-1} are denoted.

noise which is probably not true for SMEI data. To achieve a higher resolution and a more precise frequency value, the two datasets were combined into one in which we find the frequency to be 0.82215(1) d^{-1}. This is not the first time that this frequency has been reported. Smith et al. (2006) and later Henry & Smith (2012) observed this variation using a 15-year time series from the ground-based APT. These authors found a frequency of 0.82250(2) d^{-1} which has recently been revised by Smith (2019) to 0.82247(2) d^{-1}. The difference between our and their result is approximately 1.5 cycle in 12 years, which corresponds to the length of the data string, and this could explain the discrepancy.

Unfortunately, the large scatter in the data and strong aliases mean that the comparatively small amplitude of the 0.82 d^{-1} frequency is not visible in the light curve – even when the data are folded with this frequency or binned in phase.

Henry & Smith (2012) show that the amplitude varies with time. To test this finding, we split the time series into two halves for each camera. The amplitudes of the signal in the four subsets are shown in Fig. 9 along with the results from Henry & Smith (2012) for comparison. We read off the values from their Fig. 7 instead of redoing their analysis in which they performed highly sophisticated multi-level corrections for different time-dependent slow variations. For the first half of the time series, we could confidently retrieve the frequency. In the second half of the time series, the noise level of the SMEI data was too large and we have only been able to provide upper limits of the amplitude. These are calculated as three times the mean strength of all peaks in 0.2 d^{-1} frequency windows around 0.82 d^{-1}.

Although this only provides four data points, the combination with the Henry & Smith (2012) data shows very well the changing amplitude of this variation.

In the following section, we show that a new frequency of 2.48 d^{-1} is present in the BRITE data. With this knowledge, we searched for this in the SMEI data as well. From Fig. 7 it is possible that such a frequency is present at least in Camera 1 data. Camera 2 data do not show this frequency at a significant level. The 2.48 d^{-1} feature lies outside the broad (probably instrumental) bump between 2.3 and 2.4 d^{-1}. Therefore, this contamination should not be the explanation of the absence of the 2.48 d^{-1} frequency from the Camera 2 data. However, we do not have another explanation. In the combined data (Fig. 8) only a weak signal appears at the expected frequency. We find the frequency to be 2.47951(4) d^{-1}. There is no sign of this frequency in the

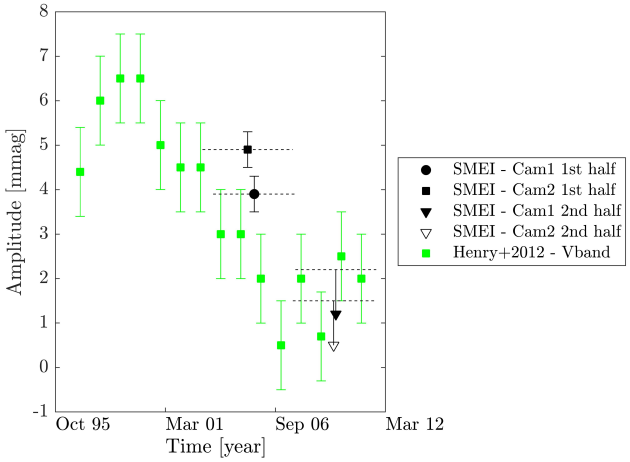

Fig. 9. Comparison of amplitudes of the 0.82 d^{-1} frequency determined in this work (SMEI) and reported by Henry & Smith (2012; APT). The two SMEI datasets were split into two subsets. The first point for each camera is a measurement of the amplitude of the signal while the second point (triangle) is an upper limit. The dashed lines indicate the time span of the two SMEI subsets. When BRITE observed the star in 2015–2018 this frequency was not recovered with a detection limit of ~1 mmag.

window function but we cannot completely disregard that it is an annual alias of the aforementioned 0.82 d^{-1} since SMEI data, in general, have strong annual trends. Nevertheless, we regard it as genuine because it is present in BRITE data. The 2.48 d^{-1} frequency was first reported by Baade et al. (2017). It was also reported for the contemporaneous APT data by Smith (2019), who, however, does not state in which time interval nor at what amplitude this is seen.

Although data from both cameras appear to have other signals as well, the only signal that possibly exists in both datasets is at 1.24583(2) d^{-1}. While clearly present in Camera 2 data, it is not certain if it is in Camera 1 data. In the combined data it appears much more significant. The 1.25 d^{-1} signal was first found by multiplying the amplitude spectra of the two cameras which emphasises signals and eliminates non-common noise spikes. We note that this is a different method than the combination of data and it was not used for analysis because it is not a reliable detection method. It only gives a first suggestion of what the two amplitude spectra have in common and any real

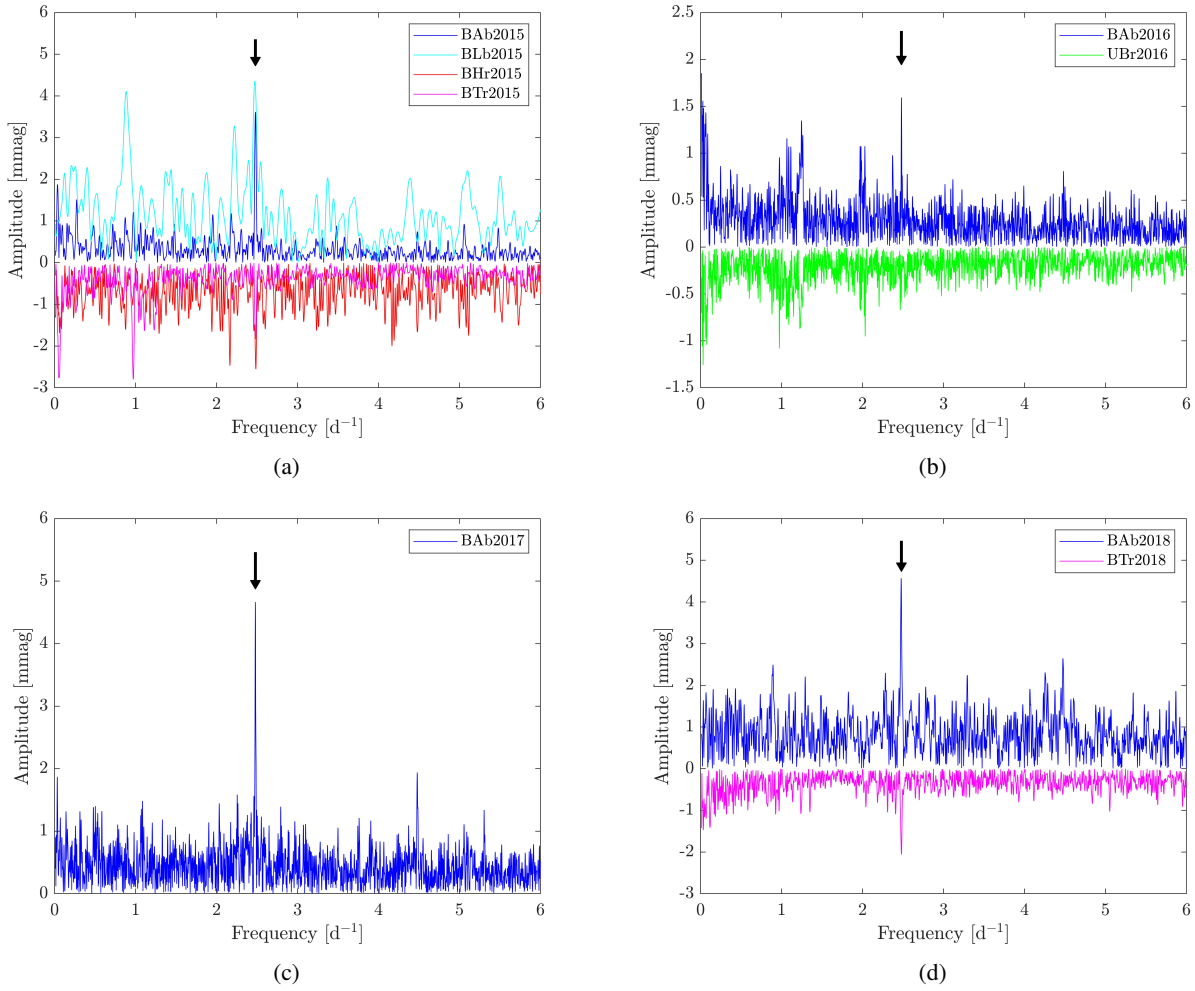

Fig. 10. Amplitude spectra for all BRITE datasets separated by satellite and season. Colours correspond to those used in Fig. 4. Data in *panel a* are from 2015, (*b*) 2016, (*c*) 2017, and (*d*) 2019. Amplitude spectra from red-filtered satellites are flipped to negative values for clarity. The arrows denote the most prominent feature at 2.48 d^{-1}.

Table 3. Frequencies and amplitudes from BRITE.

	BAb2015	BLb2015	BHr2015	BTr2015	UBr2016	BAb2016	BAb2017	BAb2018	BTr2018	Combined
Frequency [d^{-1}]	2.4802(7)	2.472(6)	2.486(2)	2.481(2)	2.478(1)	2.4809(7)	2.4797(3)	2.4773(7)	2.4799(9)	2.47936(2)
Amplitude [mmag]	3.6(3)	4.5(8)	2.8(5)	1.9(3)	0.6(2)	1.7(3)	4.5(4)	4.5(6)	2.0(3)	–

signal should show up in a plot where the spectra are multiplied. However, the latter is only a necessary and not a sufficient condition. With this method, the 0.82 d^{-1}, 1.25 d^{-1}, and 2.48 d^{-1} frequencies were clearly present while all other possible contenders disappeared.

Lastly, we searched for the orbital period of the companion in an attempt to detect photometric changes in the light curve owing to the possible spiral structure. As a consequence of the large noise levels at low frequencies, we did not find any significant signal at this frequency.

4.3. Frequencies in BRITE photometry

The amplitude spectra of the reduced and pre-whitened BRITE data can be seen in Fig. 10. The scale of the ordinate is not the same for all plots. The most prominent feature is at 2.48 d^{-1}. This variability is present in all amplitude spectra at different amplitudes. The extracted frequencies are presented in Table 3 and the amplitudes are shown in Fig. 11. The frequencies differ a little more than the 1σ uncertainty. This is likely due to the short timespan in each dataset which easily enhances the effects of non-periodic signals. However, because of the short time spans of each dataset, systematic effects may become more pronounced. The amplitude spectrum of all BRITE data as well as all the blue(red) satellites combined separately can be seen in Fig. 12. The frequency calculated for the entire (blue+red) time series is 2.47936(2) d^{-1}. The frequency found in the SMEI data is 2.47951(4) d^{-1} meaning the frequencies differ by 2.5σ. We emphasise that the noise in SMEI is possibly non-Gaussian which may affect the uncertainties. We attribute the difference between the frequencies to noise statistics.

Focussing on the amplitudes in Fig. 11, two features are noticeable: the change in amplitude over time and the difference between blue- and red-filter satellites. In seasons when the star

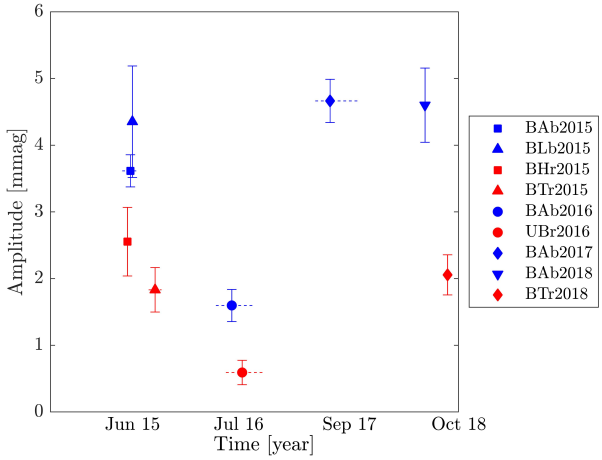

Fig. 11. Amplitudes of the 2.48 d^{-1} frequency in the BRITE data. The horizontal bars indicate the time coverage of each dataset.

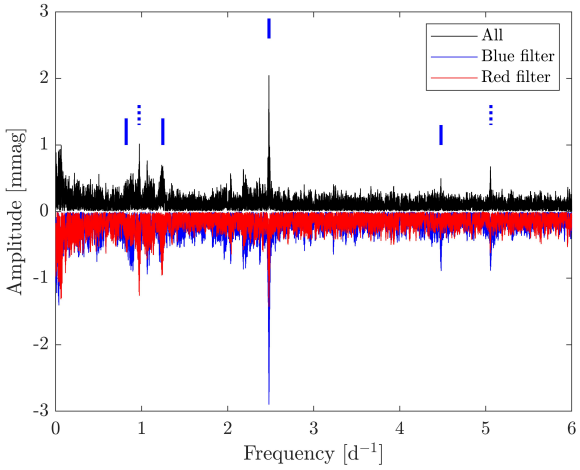

Fig. 12. Amplitude spectrum of all BRITE datasets combined in black. Blue and red filter satellite data are also combined separately and plotted with corresponding colours. Blue and red spectra are flipped to negative values for clarity. Vertical full lines indicate 0.82, 1.25, 2.48, and 4.48 d^{-1} respectively. Dotted lines indicate 0.97 and 5.06 d^{-1}, respectively.

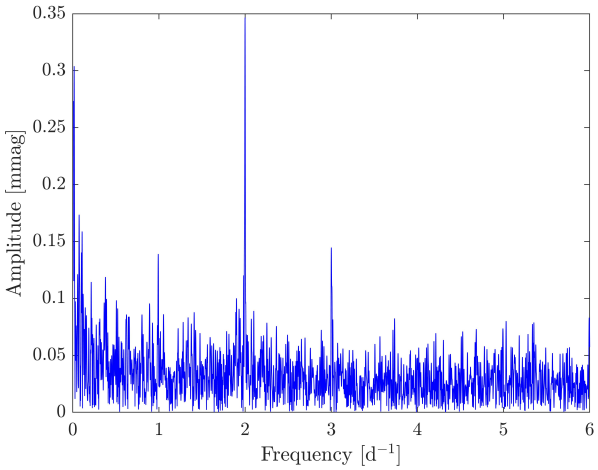

Fig. 13. Window function of BRITE dataset BAb2017.

was observed simultaneously with a blue- and red-filter satellite, the amplitude in the blue filter was larger. Therefore, this could indicate that the signal is caused by a thermal mechanism. We examined the ratio between the amplitudes and compared it to ratios between black body curves. However, the uncertainties on the amplitudes are too large and the number of data points is too small to make this viable. A more elaborate interpretation of a possible thermal nature of this frequency would be unjustifiable at this moment. The other noticeable aspect of the amplitude behaviour is the obvious fading in 2016 and recovery in 2017. Satellite BAb observed γ Cas during all four observing runs and thereby suggests that the changes in amplitude are not instrumental.

We attempted to ascribe the frequency to the primary or the companion star by examining the Doppler shifts of the peaks in the BRITE amplitude spectrum which could be attributed to the orbital velocity (see Shibahashi & Kurtz 2012, for an explanation of this principle). Unfortunately, the time series were too short (making the amplitude peaks too broad) for a conclusion to be drawn with confidence.

Furthermore, we used *Hubble* Space Telescope[4] (HST) data to look for the 2.48 d^{-1} signature in the UV region. The HST observed γ Cas with the Goddard High-Resolution Spectrograph (Brandt et al. 1994) between March 14 to 15 1996 for a total of ~20 h. These data have been extensively analysed by Smith & Robinson (1999). With the new knowledge of the 2.48 d^{-1} frequency we re-analysed these data to look for this signature but the length of the time series is insufficient to verify a detection.

There is a four-year gap between the observations with SMEI and BRITE (see Fig. 3). From SMEI it was clear that the 0.82 d^{-1} frequency was decreasing in amplitude over the observing run. In agreement with this trend, the 0.82 d^{-1} frequency is not present in any of the BRITE data (individually or combined) with a detection limit of ~1 mmag.

The amplitude spectra in Fig. 10 contain other signals that could be significant. In particular, Figs. 10c and 12 have a signal at 4.48 d^{-1}. This disappears when the data are pre-whitened for the 2.48 d^{-1} signal indicating that is just a daily alias. The 2 d^{-1} alias is also present in the window function and much stronger than both the 1 and 3 d^{-1} alias explaining why we do not detect the 3.48 d^{-1} (see Fig. 13). From the SMEI data we find that there is a possible signal at 1.25 d^{-1}. When looking at the amplitude spectrum of the full BRITE time series (Fig. 12) there is an indication that it is present in the BRITE data as well. This is, however, located in a cluster of peaks and its exact frequency could not be verified with certainty. Two other peaks are indicated by dashed lines in Fig. 12. These are located at 0.97 and 5.06 d^{-1} putting them relatively close to the daily aliases. At this point, we cannot confirm nor deny their realness.

We searched for a variation corresponding to the orbital binary period but did not find this variation. The BRITE datasets have all been shifted individually to zero, and this might have eliminated a coherent signal corresponding to the orbital period. The gaps in the data further complicate a possible detection.

Lastly, there are peaks of uncertain validity in all BRITE spectra. None of these appears to be consistent across multiple satellites and it is assumed that they are caused by effects intrinsic to the individual satellites (or other non-stellar effects).

5. Discussion

5.1. Possible spiral structure

The most remarkable feature seen in Fig. 5 is the blue versus red-asymmetric amplitude distribution in the wings of the Hα

[4] www.spacetelescope.org

emission line at the orbital frequency of the companion. The simplest explanation would be a one-armed spiral which can result from the rotational distortion of the gravity field of the B star alone (Okazaki 1991), that is without need for a companion star. In this case, depending on the sense of rotation of the disk, the concave and convex side of the arm would each only be seen at positive or negative radial velocities, respectively. Because the two sides may differ not just in geometry but also in physical properties, the stellar light could be reprocessed differently and a blue versus red asymmetry of the amplitude distribution (as in Fig. 5) would arise. The close proximity of the main feature in Fig. 5 to the orbital frequency of the companion implies that the structure is not only induced by the gravitational quadrupole moment of the B star. It would be unlikely that the frequency of the spiral structure coincided with the orbital frequency without the companion and the disk being physically linked. In many binary stars the gravitational effect of the companion is expected to dominate over the quadrupole moment of the B star, and a two-armed spiral would develop that is phase-locked to the companion, where one arm roughly points at the companion and the other one points away from the companion (Panoglou et al. 2018). If the two arms are identical and separated by 180° in disk azimuth, any photometric signal would have to occur at twice the orbital frequency. Accordingly, the absence of variability at double the orbital frequency implies deviations from this simplifying geometrically symmetric picture. Other possible reasons for not observing a signal at twice the orbital frequency are as follows: (a) the disk might not be steady (the build-up of the final spiral structure can take up to a few tens of orbits); (b) the injection of mass from the star to the disk is not isotropic; (c) the orbit is slightly eccentric; (d) orbital and disk planes are different; and/or (e) non-gravitational effects interfere, for example radiation from the companion ionises one arm more than the other. The latter effect could also affect the visibility of one arm over the other, making it hard to detect even though it might be there.

Most of these effects would lead not only to variations in the optical spectra with the orbital frequency instead of its first harmonic but also to a blue versus red asymmetry in the amplitude spectrum as observed in γ Cas (Fig. 5). Spectro-interferometry might help to downselect the number of asymmetry-causing effects such as geometry, temperature, density, and velocity.

γ Cas has been observed interferometrically several times in recent years. Most relevant for this discussion is the work by Berio et al. (1999) because they observed a one-armed structure in the disk using observations between 1988 and 1994. At that time it was not yet known that γ Cas had a companion, which could induce a two-armed spiral, but, as discussed above, the observation of only one arm does not necessarily mean that a second arm was not present. More recently, Stee et al. (2012) looked for a one-armed structure but find no evidence of such a structure. They observed γ Cas from 2008 to 2010. Because the disk varies on timescales of a few years, it is possible that the spiral structure disappeared at some point between 1994 and 2008. This also means that, even though no spiral was observed in 2010, it can exist today, as the results from our spectroscopic analysis suggest.

5.2. Possible disk truncation

The relative stability of the Hα profiles indicates that the star has not had any large outburst in recent years. If the mass loss had ceased, the inner disk would re-accrete and the outer regions dissipate with time. The timescale for dissipation depends on various parameters, for example outburst rate, mass outflow rate, and viscosity, but is of the order of a year or less (Ghoreyshi et al. 2018). However, the disk has been present over a number of years (according to the BeSS database at least from 2006 to 2017, see Fig. 1) and does not seem to be disappearing. The disk is therefore likely being regularly replenished but since this only happens in the inner parts of the disk, the overall structure of Hα is roughly constant. The inner parts may also restore structure more quickly and since the observed variability is mostly at high velocities (inner parts) this could further contribute to the apparent stability of the Hα line. An explanation for this quiet nature could be linked to the influence of the companion on the disk. From the flat top profile and the orbital frequency found in the disk (as opposed to its harmonics, see Sect. 4.1), it is evident that the companion does have a strong effect on the disk.

Outbursts are typical of Be stars (e.g. Bernhard et al. 2018; Labadie-Bartz et al. 2017). Probably, they are the (main) mechanism through which these stars build and sustain their disks. Panoglou et al. (2016) also show that the truncation by the companion can limit the mass flow across the truncation radius. It is possible that if the Be star ejects sufficient amounts of matter and if the disk cannot grow past the truncation radius, it might become thicker instead of wider. If the inner region becomes dense enough to be optically thick, the outbursts would no longer cause a brightening, meaning that the seemingly stable nature of the disk is not due to the absence of outbursts. If this is the case, it is also possible that continued growth of the disk in geometrical thickness could cause it to enter our line of sight. Shell lines can then occur as a consequence of the absorption of light from the innermost parts of the disk. This could explain why in the 1930s, γ Cas displayed a shell phase right after large outbursts (Harmanec 2002, and references therein) despite the 45° inclination (Quirrenbach et al. 1997) of the disk.

In general three mechanisms seem to be able to cause the line profile structure of the Be stars to change between wine-bottle structure and shell phase. One is the above-mentioned varying geometrical thickness of the disk. The second is a varying viewing aspect (i.e. azimuth) angle of the disk as is shown in simulations by Panoglou et al. (2018). Thirdly, if the star has a companion with a misaligned orbit, this causes the disk to precess and thereby, more or less periodically, enter our line of sight. This is, for example, the case for the Be star Pleione (Hirata 2007). It has not been shown that γ Cas's disk is (or is not) precessing. If it is not precessing, the mass build-up of the disk might be an explanation for the appearance of shell components in the Hα profiles.

5.3. Possible non-radial pulsation

We recovered the $0.82\,\mathrm{d}^{-1}$ frequency found by Smith et al. (2006) and Henry & Smith (2012) using data from the SMEI satellite. The frequency was observed from 2003 to 2011, and in this time frame, it faded in amplitude until it became undetectable. We show that when the star was observed again in 2015 with BRITE, the $0.82\,\mathrm{d}^{-1}$ frequency was still undetectable but a new frequency of $2.48\,\mathrm{d}^{-1}$ now dominates.

Smith et al. (2006) ascribed the $0.82\,\mathrm{d}^{-1}$ frequency to the rotation of the primary star. Their main argument for doing so was a match with expected values for the rotation rate. From radial velocity measurements and stellar interferometry, they estimated the rotation period to be 1.08−1.41 days ($0.71-0.93\,\mathrm{d}^{-1}$) corresponding with the observed 1.21 day period ($0.82\,\mathrm{d}^{-1}$). The other plausible contender in the explanation was NRP. This was disregarded because, according to Henry & Smith (2012), there was no evidence of NRPs of the order of one day in early-type Be stars known at the time.

This occurred despite the existence of works such as that of Rivinius et al. (2003). A few years later CoRoT discovered NRPs on these timescales in many O9-B1.5-type stars (e.g. Degroote et al. 2009; Briquet et al. 2011). This was acknowledged by Henry & Smith (2012), but they argued that these studies are for slow or intermediate rotators and cannot necessarily be applied to the rapidly rotating B star in γ Cas. However, since then, periods of the order of one day were found in several other very early-type Be stars (e.g. Baade et al. 2017; Semaan et al. 2018). At this time it seems much more likely for Be stars to have NRPs than not.

Although γ Cas is a rapid rotator, 2.48 d^{-1} interpreted as rotation frequency would lead to surface velocities larger than the break-up velocity (near-critical rotation is at 0.71–0.93 d^{-1}; Smith et al. 2006) so that any rotational interpretation is impossible. Potentially the 2.48 d^{-1} frequency could be due to the rotation of the secondary. The amplitudes (for both frequencies) are, however, unexpectedly large for a companion that is already greatly outshined by the primary in the sensitivity range of BRITE. For this reason, we assume that both frequencies are associated with the primary and that the 2.48 d^{-1} frequency is not a rotational signature.

The ratios between the two frequencies are calculated using combinations of the values found in Table 4. When both frequencies are from SMEI the ratio is 3.01588(5); from SMEI and BRITE the ratio is 3.01570(4) and from APT and BRITE the ratio is 3.01453(8). Although these differ slightly they are all significantly different from 3, excluding the possibility that these are just harmonics. As mentioned, the uncertainties of the frequencies are calculated with one of the most widely used tools of the field (i.e. Period04) (Lenz & Breger 2005).

Although SMEI and BRITE are very different satellites, the uncertainties of the frequencies from these satellites are of the same order of magnitude when the BRITE data are combined. On the one hand, this is because of the higher signal-to-noise ratio of the BRITE data and, on the other hand, because of the longer time baseline of the SMEI data, which happen to balance out. It should be noted that the uncertainties provided in this work assume that the noise is normally distributed, which may not be the case for SMEI. They also do not take systematics into account. Therefore, for a more conservative estimate, we combine the SMEI/SMEI and BRITE/SMEI to a ratio of 3.0158(1). This is still far from 3 and we conclude that the 0.82 d^{-1} and 2.48 d^{-1} frequencies are not related. Since they are not harmonics and not both due to rotation, the most likely origin is NRPs.

A further indication of multi-frequency NRP is the 1.25 d^{-1} frequency. Although not as prominent as the other two frequencies, the detection of this signal in two independent datasets (SMEI and BRITE) enhances its significance and supports the NRP nature of all three signals. The ratio of 2.48 d^{-1} to 1.25 d^{-1} is 1.99025(5), which is close to 2, but differs to within the nominal uncertainties. Even in the case that we greatly underestimate the uncertainties and the harmonic relations are real, either 2.48 d^{-1} is the independent frequency or both 1.25 d^{-1} and 0.82 d^{-1} are independent. This is so because, in that case, the only frequency that can be the parent of all three variations is 2.48 d^{-1}. At a ratio of ~1.5, 1.25 d^{-1} and 0.82 d^{-1} are not harmonics. Therefore, if one of the two is independent, so is the other. In either case, the two higher frequencies fall into the domain of NRP frequencies observed in other Be stars but are far outside the range of rotation. There may be further signals present in the star but more data are needed to verify this.

Nearly all Be stars are observed to have NRPs (e.g. Rivinius et al. 2003) so it is not surprising to see them in γ Cas.

Table 4. Frequencies from SMEI, APT and BRITE; APT result from Smith (2019).

	SMEI	APT	BRITE
Frequency [d^{-1}]	0.82215(1)	0.82247(2)	
	1.24583(2)		
	2.47951(4)		2.47936(2)

Furthermore, the interaction of multiple NRP modes may be the driving agent of the star-to-disk mass-transfer events (outbursts) in Be stars (e.g. Baade et al. 2018a,b) for which the magnetic model of Smith and coworkers does not offer an alternative explanation.

6. Conclusions

We have confirmed the 0.82215(1) d^{-1} frequency (1.21 day period) first presented by Smith et al. (2006) and Henry & Smith (2012). Using SMEI with a long time baseline, we showed that this frequency is present from 2003 to 2011 with decreasing amplitude. The BRITE photometry from 2015 to 2019 supports the disappearance of this frequency with a detection limit of ~1 mmag. In BRITE data, we found a dominant signal at a frequency of 2.47936(2) d^{-1} (period of 0.4 days). From re-analysis of the SMEI data, it appear possible that this 2.48 d^{-1} signal was already present at some point between 2003 and 2011. Since the 2.48 d^{-1} variation cannot be due to rotation, a common origin would impact the interpretation that the 1.21 day variation is the rotational signature. If they are of the same nature they would most likely be NRPs. The fact that nearly all Be stars are observed to have NRPs strengthens this explanation. If neither the 2.48 d^{-1} nor the 0.82 d^{-1} signals are NRP frequencies, γ Cas would be a highly unusual Be star for which no plausible explanation for these frequencies (or at least the higher frequency) exists. The possible detection of a 1.24583(4) d^{-1} frequency in both SMEI and BRITE data would further enhance this conclusion. It was shown that at least the 0.82 d^{-1} and 1.25 d^{-1} frequencies or the 2.48 d^{-1} frequency is independent which still favours a NRP interpretation over a rotational interpretation.

With γ Cas being a very bright star, the NRP question can probably be settled through a high-cadence series of high-quality spectra. Such data could also unambiguously answer the question of whether the migrating sub-features (Yang et al. 1988) in line profiles are due to a pulsational velocity field or absorbing cloudlets. We note that, in the case of Spica (a rapidly rotating B1 star without emission lines), Smith (1985) has, in contrast to γ Cas, advocated NRP as the explanation of migrating sub-features. Apart from Spica not having the risk of contamination from circumstellar material, there does not seem to be a basic qualitative difference between these variations in γ Cas and Spica. For such an analysis, the time series must cover at least a half dozen rotational periods to enable a significant identification. The time span of the HST observations was too short (see Sect. 4.3) for this, which we confirmed with our time series analysis of these data. If at the time of such future observations the 0.82 d^{-1} variability has come back, the spectra might also identify what physical property is modulating the light.

A periodic aspect change of the spiral arms of the disk was identified in the variability of the Hα emission profile, corresponding to the orbital frequency. Remarkably, the amplitude distribution with wavelength of this frequency displayed a blue versus red asymmetry. We discussed how this could be caused by a spiral structure in the disk in phase with the

companion. Owing to different opacities, the concave and convex parts of the spiral could reprocess the stellar light differently. This could give rise to a different brightness when the arm is moving towards (blue) and away (red) from the observer which could produce such an asymmetry. It was, however, not possible to conclude if the spiral structure is one- or two-armed. If the spiral has two arms, the absence of a significant feature at twice the orbital frequency in the amplitude spectrum shows that any two arms are not symmetric in orbital phase and/or strength. Future observational experiments might try to address these questions more specifically.

Acknowledgements. We would like to thank the referee Dr. Joachim Puls for carefully reviewing the manuscript and suggesting changes that have improved the quality of the paper. This work is based on CB's Master Thesis "Variability of the Former Prototype Be star and X-ray Binary γ Cassiopeiae" (October 2018, Ludwig Maximilian University of Munich, unpublished). The authors thank the BRITE operations staff for their untiring efforts to deliver data of the quality that enabled this investigation. The authors thank Dr. Bernard Jackson for providing the SMEI data with camera identification which made it possible to improve this work. This work has made use of the BeSS Database, operated at LESIA, Observatoire de Meudon, France: http://basebe.obspm.fr. This research has made use of NASA's Astrophysics Data System (ADS). This research has made use of the SIMBAD database, operated at CDS, Strasbourg, France. CB thanks the European Southern Observatory as well as the Max Planck Institute for Astrophysics for hosting her during this research. CB acknowledges financial support from Knud Højgaards Fond (grant: 16-01-2164), Dansk Tennis Fond, Nordea-fonden (grant: 01-2016-001046) and Oticon Fonden (grant: 16-3182). Funding for the Stellar Astrophysics Centre is provided by The Danish National Research Foundation (Grant agreement no.: DNRF106). DP acknowledges financial support from Conselho Nacional de Desenvolvimento Científico e Tecnológico (Brazil) through grant 300235/2017-8. APi acknowledges support from the NCN grant no. 2016/21/B/ST9/01126. AFJM is grateful for financial aid from NSERC (Canada) and FQRNT (Quebec). GAW also acknowledges NSERC (Canada). GH acknowledges support from the NCN grant 2015/18/A/ST9/00578. APo was responsible for image processing and automation of photometric routines for the data registered by BRITE-nanosatellite constellation, and was supported by Rector Grant no. 02/140/RGJ20/0001.

References

Abt, H. A., & Levy, S. G. 1978, ApJS, 36, 241
Baade, D. 1988, in The Impact of Very High S/N Spectroscopy on Stellar Physics, eds. G. Cayrel de Strobel, & M. Spite, IAU Symp., 132, 217
Baade, D., Rivinius, T., Pigulski, A., et al. 2017, in Second BRITE-Constellation Science Conference: Small satellites – Big Science, eds. K. Zwintz, & E. Poretti, Proc. Pol. Astron. Soc., 5, 196
Baade, D., Pigulski, A., Rivinius, T., et al. 2018a, A&A, 610, A70
Baade, D., Rivinius, T., Pigulski, A., et al. 2018b, in 3rd BRITE Science Conference, eds. G. A. Wade, D. Baade, J. A. Guzik, & R. Smolec, 8, 69
Balbus, S. A. 2003, ARA&A, 41, 555
Baldwin, R. B. 1940, ApJ, 92, 82
Berio, P., Stee, P., Vakili, F., et al. 1999, A&A, 345, 203
Bernhard, K., Otero, S., Hümmerich, S., et al. 2018, MNRAS, 479, 2909
Brandt, J. C., Heap, S. R., Beaver, E. A., et al. 1994, PASP, 106, 890
Breger, M., Handler, G., Garrido, R., et al. 1999, A&A, 349, 225
Briquet, M., Aerts, C., Baglin, A., et al. 2011, A&A, 527, A112
Buffington, A., Bisi, M. M., Clover, J. M., Hick, P. P., & Jackson, B. V. 2007, AGU Fall Meeting Abstracts, SH33A
Carciofi, A. C., Bjorkman, J. E., Otero, S. A., et al. 2012, ApJ, 744, L15
Collins, II, G. W. 1987, in IAU Colloq. 92: Physics of Be Stars, eds. A. Slettebak, & T. P. Snow, 3
Degroote, P., Aerts, C., Ollivier, M., et al. 2009, A&A, 506, 471
de Mink, S. E., Langer, N., & Izzard, R. G. 2011, Bull. Soc. R. Sci. Liege, 80, 543
de Mink, S. E., Langer, N., Izzard, R. G., Sana, H., & de Koter, A. 2013, ApJ, 764, 166
Ekström, S., Meynet, G., Maeder, A., & Barblan, F. 2008, A&A, 478, 467
Frandsen, S., Jones, A., Kjeldsen, H., et al. 1995, A&A, 301, 123
Frémat, Y., Zorec, J., Hubert, A.-M., & Floquet, M. 2005, A&A, 440, 305
Ghoreyshi, M. R., Carciofi, A. C., Rímulo, L. R., et al. 2018, MNRAS, 479, 2214
Goss, K. J. F., Karoff, C., Chaplin, W. J., Elsworth, Y., & Stevens, I. R. 2011, MNRAS, 411, 162
Granada, A., Ekström, S., Georgy, C., et al. 2013, A&A, 553, A25
Güdel, M., & Nazé, Y. 2009, A&ARv, 17, 309
Hanuschik, R. W. 1986, A&A, 166, 185
Hanuschik, R. W. 1995, A&A, 295, 423
Hanuschik, R. W., Hummel, W., Sutorius, E., Dietle, O., & Thimm, G. 1996, A&AS, 116, 309
Harmanec, P. 2002, in Exotic Stars as Challenges to Evolution, eds. C. A. Tout, & W. van Hamme, ASP Conf. Ser., 279, 221
Harmanec, P., Habuda, P., Štefl, S., et al. 2000, A&A, 364, L85
Heard, J. F. 1938, J. R. Astron. Soc. Can., 32, 353
Henry, G. W., & Smith, M. A. 2012, ApJ, 760, 10
Hick, P., Buffington, A., & Jackson, B. V. 2005, in Solar Physics and Space Weather Instrumentation, eds. S. Fineschi, & R. A. Viereck, Proc. SPIE, 5901, 340
Hick, P., Buffington, A., & Jackson, B. V. 2007, Proc. SPIE, 6689, 66890C
Hirata, R. 2007, in Active OB-Stars: Laboratories for Stellare and Circumstellar Physics, eds. A. T. Okazaki, S. P. Owocki, & S. Stefl, ASP Conf. Ser., 361, 267
Horne, K., & Marsh, T. R. 1986, MNRAS, 218, 761
Jackson, B. V., Buffington, A., Hick, P. P., et al. 2004, Sol. Phys., 225, 177
Jaschek, M., Slettebak, A., & Jaschek, C. 1981, Be Star Newsletter, 4, 9
Jernigan, J. G. 1976, IAU Circ., 2900, 2
Kato, S. 1983, PASJ, 35, 249
Kjeldsen, H. 1992, PhD Thesis, University of Aarhus, Denmark
Kříž, S., & Harmanec, P. 1975, Bull. Astron. Inst. Czech., 26, 65
Krtička, J., Owocki, S. P., & Meynet, G. 2011, A&A, 527, A84
Labadie-Bartz, J., Pepper, J., McSwain, M. V., et al. 2017, AJ, 153, 252
Langer, N., Baade, D., Bodensteiner, J., et al. 2020, A&A, 633, A40
Lee, U., Osaki, Y., & Saio, H. 1991, MNRAS, 250, 432
Lenz, P., & Breger, M. 2005, Commun. Asteroseismol., 146, 53
Meilland, A., Millour, F., Kanaan, S., et al. 2012, A&A, 538, A110
Miroshnichenko, A. S., Bjorkman, K. S., & Krugov, V. D. 2002, PASP, 114, 1226
Montgomery, M. H., & O'Donoghue, D. 1999, Delta Scuti Star Newsletter, 13, 28
Nazé, Y., & Motch, C. 2018, A&A, 619, A148
Neiner, C., de Batz, B., Cochard, F., et al. 2011, AJ, 142, 149
Nemravová, J., Harmanec, P., Koubský, P., et al. 2012, A&A, 537, A59
Okazaki, A. T. 1991, PASJ, 43, 75
Okazaki, A. T., Bate, M. R., Ogilvie, G. I., & Pringle, J. E. 2002, MNRAS, 337, 967
Oudmaijer, R. D., & Parr, A. M. 2010, MNRAS, 405, 2439
Owocki, S. P., Cranmer, S. R., & Blondin, J. M. 1994, Ap&SS, 221, 455
Pablo, H., Whittaker, G. N., Popowicz, A., et al. 2016, PASP, 128, 125001
Panoglou, D., Carciofi, A. C., Vieira, R. G., et al. 2016, MNRAS, 461, 2616
Panoglou, D., Faes, D. M., Carciofi, A. C., et al. 2018, MNRAS, 473, 3039
Papaloizou, J. C., Savonije, G. J., & Henrichs, H. F. 1992, A&A, 265, L45
Pigulski, A. 2018, in 3rd BRITE Science Conference, eds. G. A. Wade, D. Baade, J. A. Guzik, & R. Smolec, 8, 175
Pols, O. R., Cote, J., Waters, L. B. F. M., & Heise, J. 1991, A&A, 241, 419
Popowicz, A., Pigulski, A., Bernacki, K., et al. 2017, A&A, 605, A26
Pringle, J. E. 1981, ARA&A, 19, 137
Puls, J., Vink, J. S., & Najarro, F. 2008, A&ARv, 16, 209
Quirrenbach, A., Bjorkman, K. S., Bjorkman, J. E., et al. 1997, ApJ, 479, 477
Rímulo, L. R., Carciofi, A. C., Vieira, R. G., et al. 2018, MNRAS, 476, 3555
Rivinius, T., Štefl, S., & Baade, D. 1999, A&A, 348, 831
Rivinius, T., Baade, D., & Štefl, S. 2003, A&A, 411, 229
Rivinius, T., Carciofi, A. C., & Martayan, C. 2013, A&ARv, 21, 69
Secchi, A. 1866, Astron. Nachr., 68, 63
Semaan, T., Hubert, A. M., Zorec, J., et al. 2018, A&A, 613, A70
Shakura, N. I., & Sunyaev, R. A. 1973, A&A, 24, 337
Shibahashi, H., & Kurtz, D. W. 2012, MNRAS, 422, 738
Smith, M. A. 1985, ApJ, 297, 206
Smith, M. A. 2019, PASP, 131, 044201
Smith, M. A., & Robinson, R. D. 1999, ApJ, 517, 866
Smith, M. A., Robinson, R. D., & Corbet, R. H. D. 1998, ApJ, 503, 877
Smith, M. A., Henry, G. W., & Vishniac, E. 2006, ApJ, 647, 1375
Stee, P., Delaa, O., Monnier, J. D., et al. 2012, A&A, 545, A59
Štefl, S., Okazaki, A. T., Rivinius, T., & Baade, D. 2007, in Active OB-Stars: Laboratories for Stellare and Circumstellar Physics, eds. A. T. Okazaki, S. P. Owocki, & S. Stefl, ASP Conf. Ser., 361, 274
Struve, O. 1931, ApJ, 73, 94
Tokovinin, A. A. 1997, A&AS, 124, 75
Wade, G. A., Petit, V., Grunhut, J. H., Neiner, C., & MiMeS Collaboration 2016, in Bright Emissaries: Be Stars as Messengers of Star-Disk Physics, eds. T. A. A. Sigut, & C. E. Jones, ASP Conf. Ser., 506, 207
Webb, D. F., Mizuno, D. R., Buffington, A., et al. 2006, J. Geophys. Res. (Space Phys.), 111, A12101
Weiss, W. W., Rucinski, S. M., Moffat, A. F. J., et al. 2014, PASP, 126, 573
Wenger, M., Ochsenbein, F., Egret, D., et al. 2000, A&AS, 143, 9
White, N. E., Swank, J. H., Holt, S. S., & Parmar, A. N. 1982, ApJ, 263, 277
Yang, S., Ninkov, Z., & Walker, G. A. H. 1988, PASP, 100, 233